

## NOTE

## Measuring Corner Properties

Paul L. Rosin

*Department of Information Systems and Computing, Brunel University, Middlesex, United Kingdom*

E-mail: Paul.Rosin@brunel.ac.uk

Received June 8, 1998; accepted July 10, 1998

**We describe methods to measure the following properties of gray level corners: subtended angle, orientation, contrast, bluntness (or rounding of the apex), and boundary curvature (for cusps). Unlike most of the published methods for extracting these properties these new methods are relatively simple, efficient, and robust. They rely on the corner being pre-detected by a standard operator, thus making the measurement problem more tractable. Using 13,000 synthetic images the methods are assessed over a range of conditions: corners of varying orientations and subtended angles, as well as different degrees of noise.** © 1999 Academic Press

## 1. INTRODUCTION

The three most commonly used features in computer vision are regions, edges, and corners. Whereas regions are normally attributed properties to make them useful as input for subsequent processing stages such as matching, little except for strength was extracted by early edge and corner detectors, e.g., [11, 20], not to mention more recent ones, e.g., [5, 21]. Being sparse features, their mere presence was considered sufficiently informative. However, over the past few years more attention has started to be paid to the properties of edges and corners too. The reason for attributing corners with ever more properties is that they then provide much richer descriptions, thereby making them more effective features. For instance, in tracking, model matching, or model indexing, corner properties are capable of constraining the corner correspondences either as unary constraints or  $n$ -ary constraints between several corners. The latter enables viewpoint invariance. For example, under orthographic projection selected pairs of coplanar corners may be expected to have identical, but unknown, subtended angles or orientations. In [17] we demonstrated how the addition of relative color and subtended angle corner properties (binary and unary constraints, respectively) enabled the number of arcs in the association graph to be drastically reduced (by almost two orders of magnitude) in a model recognition application using maximal clique graph matching. In that paper and this we restrict our attention to L-corners. Examples of analyses of higher order corners are given by Deriche [8] and Rohr [15].

Recent examples of edge properties being measured are scale [3], diffuseness, height, and width [22]. Regarding corners, several interesting methods have been developed recently to measure scale, orientation, subtended angle, contrast, and blurring [2, 4, 10, 12, 15, 16]. However, a problem with these techniques is that they tend to be complex, iterative, and/or require second order partial derivatives, which impacts on both their efficiency and reliability. In contrast, rather than attempt the complicated task of simultaneously detecting and describing corners, in a previous paper we decoupled these two stages [17]. Standard algorithms were used to identify corner locations, and simple noniterative methods were then sufficient for extracting corner properties. Many of the techniques we developed were based on local intensity or orientation histograms generated in the corner's neighborhood. Before corner properties could be measured the histograms were smoothed by an automatically determined amount and the two main peaks located. A weakness of this approach is that it depends on correctly locating the peaks, which in turn depends on the appropriate level of smoothing being correctly determined. In this paper we develop further techniques for measuring corner properties more directly without recourse to histograms. By eliminating one potential source of error this has the potential for improving reliability and accuracy. In addition to the previously extracted corner properties we describe methods for measuring bluntness (or degree of rounding of the apex) and boundary shape (i.e., straight or curved sides).

## 2. MEASURING PROPERTIES

## 2.1. Contrast and Subtended Angle

Ghosal and Mehrotra [9] showed how Zernicke moments could be employed to recover many properties of corners and edges. Here we use the standard moments which are simpler to compute to determine corner properties in a similar manner to Tsai's [19] image thresholding scheme. We define the moments of the image intensities  $I(x, y)$  as

$$m_p = \iint I(x, y)^p dx dy$$

which we calculate within a circular window about the corner. Disregarding spatial information we model the corner in one dimension by two constant populations of gray levels  $b$  and  $d$  (bright and dark) containing  $m$  and  $n - m$  elements, respectively. The model's moments are

$$\begin{aligned} m_p &= \int_0^m b^p dt + \int_m^n d^p dt \\ &= mb^p + (n - m)d^p, \end{aligned}$$

where  $n$  is the number of pixels in the window. The required parameters are obtained using the method of moments. Taking the first three moments the resulting set of simultaneous equations can be solved to determine the values of the background and foreground intensities,

$$\begin{aligned} b &= \frac{m_1 m_2 - n m_3 + t}{2(m_1^2 - n m_2)} \\ d &= \frac{m_1 m_2 - n m_3 - t}{2(m_1^2 - n m_2)}, \end{aligned}$$

where

$$t = \sqrt{-3m_1^2 m_2^2 + 4m_1^3 m_3 + 4m_2^3 n - 6m_1 m_2 m_3 n + m_3^2 n^2}.$$

Since  $b > d$  the contrast is

$$c = b - d = \frac{t}{(m_1^2 - n m_2)}.$$

To find the subtended angle we use the fractions of the foreground and background populations within the window:  $\frac{m}{n}$  and  $\frac{n-m}{n}$ . This is the same approach that we previously described for the thresholding method [17] (although we determined contrast differently by thresholding first and then applying some postprocessing). The first moment is

$$m_1 = mb + (n - m)d$$

so that we solve for  $m$  by

$$\begin{aligned} m &= \frac{m_1 - nd}{b - d} = \frac{m_1 - nd}{c} \\ &= \left( (m_1^2 - n m_2) m_1 - \frac{n}{2} (m_1 m_2 - n m_3 - t) \right) / t. \end{aligned}$$

Assuming that the subtended angle lies in  $[0, 180)$  it is simply calculated as

$$\theta = \min\left(\frac{m}{n}, \frac{n - m}{n}\right) \times 360^\circ.$$

## 2.2. Orientation

**2.2.1. Intensity centroid.** Using standard moments it is straightforward to determine the corner orientation (without having to use the method of moments). Defining the moments as

$$m_{pq} = \sum_{x,y} x^p y^q I(x, y)$$

the centroid is then determined as

$$\mathbf{C} = \left( \frac{m_{10}}{m_{00}}, \frac{m_{01}}{m_{00}} \right).$$

Assuming the coordinate frame has been set so that the image window containing the corner is centered at the origin  $\mathbf{O}$ , the corner orientation is the angle of the vector  $\mathbf{OC}$  with a  $180^\circ$  correction to cater for corners which are darker than their background:

$$\phi = \begin{cases} \tan^{-1} \frac{m_{01}}{m_{10}} & \text{if color = bright} \\ \tan^{-1} \frac{m_{01}}{m_{10}} + 180^\circ & \text{if color = dark} \end{cases}$$

**2.2.2. Gradient centroid.** Rather than use the moments of the image intensities it is possible to use the moments of the intensity gradient magnitude  $G(x, y)$  instead:

$$\phi = \tan^{-1} \frac{\sum_{x,y} y G(x, y)}{\sum_{x,y} x G(x, y)}.$$

Although this requires the additional stage of edge detection (we use the Sobel operator to calculate  $G(x, y)$ ) it has the advantage that unlike the intensity centroid method no special care needs to be made concerning bright and dark corners, eliminating the need to predetermine corner color (as was necessary for the intensity centroid method).

**2.2.3. Symmetry.** Another method for determining corner orientation is based on the symmetry of simple corners. This implies that the orientation maximizing symmetry will coincide with the corner orientation. In a similar vein, Ogawa [13] detected corners (i.e., dominant points) of curves by measuring local symmetry. We measure corner symmetry by requiring that intensities on either side of the corner bisector should be equal. This is implemented by rotating the image window by the hypothesized orientation  $\phi$  using bilinear interpolation to obtain  $I_\phi(x, y)$ . Corner orientation can then be found as the rotation angle that minimizes the summed absolute differences in corresponding intensity values:

$$\hat{\phi} = \min_{\phi} \sum_{y=0}^W \sum_{x=-W}^W |I_\phi(x, y) - I_\phi(x, -y)|.$$

Since noise, quantization, and the process of image rotation will introduce local errors we also consider differencing not

individual pixel values but sums of row intensities,

$$\hat{\phi} = \min_{\phi} \sum_{y=0}^W \left| \sum_{x=-W}^W I_{\phi}(x, y) - \sum_{x=-W}^W I_{\phi}(x, -y) \right|,$$

or the two sums of all intensities on either side of the bisector,

$$\hat{\phi} = \min_{\phi} \left| \sum_{y=-W}^0 \sum_{x=-W}^W I_{\phi}(x, y) - \sum_{y=0}^W \sum_{x=-W}^W I_{\phi}(x, -y) \right|.$$

Of course, both  $\phi$  and  $\phi + 180^\circ$  will give the same symmetry value. Therefore we obtain an initial estimate using any of one of the techniques that we described above and then refine this by searching over a small range of orientations (e.g.,  $\pm 45^\circ$ ) to minimize the symmetry measure. Note that unlike the methods above we can use a square rather than circular window for convenience.

### 2.3. Bluntness

Corner detectors usually assume that the corners are perfectly sharp (i.e., pointed). Not only is this invalidated by noise, blurring, and quantization, but objects—both natural and man-made—often have rounded corners. Few detectors explicitly cater for this (but see Davies [6]) and none measure the degree of rounding or bluntness of the corner.<sup>1</sup>

**2.3.1. Kurtosis.** One possible way to measure bluntness is to use the statistical measure of kurtosis which quantifies the “peakness” of a distribution. It is defined using central moments as

$$\kappa = \frac{\mu_4}{\mu_2^2}.$$

Assuming the corner orientation has already been found using one of the previously described techniques we generate the projection of the image window along the direction of the corner orientation; see Fig. 1. We first rotate the image window by  $-\phi$  using bilinear interpolation as before to align the corner along the  $X$  axis, and the projection is then given by

$$P_{\phi}(y) = \sum_x I_{\phi}(x, y).$$

Before calculating kurtosis the projection function is shifted so as to zero the tails

$$P'_{\phi}(y) = P_{\phi}(y) - \min_y P_{\phi}(y).$$

Furthermore, because high order moments are being used, kurtosis is very sensitive to noise. As a precaution small values of

<sup>1</sup> In the related field of corner detection in curves there has historically been more attention paid to greater subtleties in shape (e.g., the curvature primal sketch [1]), which multiscale analysis to detect coarse as well as fine corners is much more common [7].

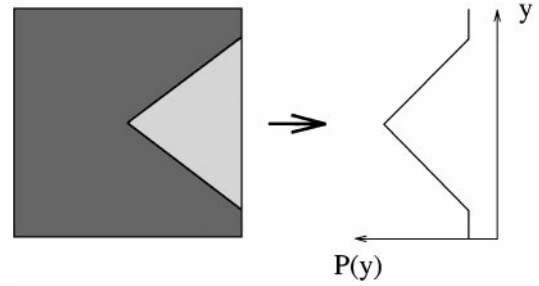


FIG. 1. Projection of image window along corner orientation.

$P'_{\phi}(y)$  are zeroed:

$$P''_{\phi}(y) = \begin{cases} P'_{\phi}(y) & \text{if } P'_{\phi}(y) > \tau \max_y P'_{\phi}(y) \\ 0 & \text{otherwise,} \end{cases}$$

where  $\tau \in [0, 1]$  is a threshold we have set to 0.1.

We can analytically determine expected values of kurtosis for simple distributions. For example, a suitable model for a perfectly sharp corner aligned on the  $Y$  axis and centered on the origin (eliminating  $m_1$ ) is the following triangular function:

$$f(x) = \begin{cases} -ax + b & \text{if } x \geq 0 \\ ax - b & \text{otherwise.} \end{cases}$$

Since the function is symmetric about  $x = 0$  we need only consider one quadrant ( $x, y > 0$ ), giving

$$\kappa = \frac{\int_0^{b/a} \frac{f(x)}{A} x^4 dx}{\left( \int_0^{b/a} \frac{f(x)}{A} x^2 dx \right)^2} = \frac{12}{5} = 2.4,$$

where

$$A = \int_0^{b/a} f(x) dx = \frac{b^2}{2a}.$$

In a similar manner a blunt corner can be roughly modeled by a parabola aligned on the  $Y$  axis and centered on the origin:

$$f(x) = -ax^2 + b.$$

Integrating over the positive  $Y$  portion of the function gives

$$\kappa = \frac{\int_{-\sqrt{\frac{b}{a}}}^{\sqrt{\frac{b}{a}}} \frac{f(x)}{A} x^4 dx}{\left( \int_{-\sqrt{\frac{b}{a}}}^{\sqrt{\frac{b}{a}}} \frac{f(x)}{A} x^2 dx \right)^2} = \frac{15}{7} \approx 2.143,$$

where

$$A = \int_{-\sqrt{\frac{b}{a}}}^{\sqrt{\frac{b}{a}}} f(x) dx = \frac{4b}{3} \sqrt{\frac{b}{a}}.$$

The extreme case of rounding in the limit as the subtended angle tends to zero is a semicircle,

$$f(x) = \sqrt{r^2 - x^2},$$

giving

$$\kappa = \frac{\int_{-r}^r \frac{f(x)}{A} x^4 dx}{\left(\int_{-r}^r \frac{f(x)}{A} x^2 dx\right)^2} = 2,$$

where

$$A = \int_{-r}^r f(x) dx = \frac{\pi r^2}{2}.$$

Thus it can be seen that rounding the corner decreases the value of the measured kurtosis. Also note that the measure is invariant to the subtended angle (which is a function of  $a$  in the above equations). For convenience we normalize the measure as  $\kappa_N = \frac{\kappa - 2}{0.4}$  to return an expected value in the range  $[0, 1]$ .<sup>2</sup>

**2.3.2. Model fitting.** A more direct way to measure corner bluntness is to fit a parametric model to the pixels in the image window. Rather than perform multivariate fitting (e.g., Rohr [15]) we assume that most of the corner properties have already been determined by other simpler methods such as those we have already described. This allows a one-dimensional fit for bluntness to be carried out that is both efficient (even without the use of partial derivatives) and robust. In particular, we require orientation, subtended angle, and foreground and background intensities to be known. This enables the image window to be rotated to align the corner with the X axis, and the model is then fitted using Brent's method [14] to minimize

$$\sum_{x=0}^W \sum_{y=-W}^W |I(x, y) - \text{corner}(x, y, p)|$$

to obtain the value of the parameter  $p$ .

We model a rounded corner by a hyperbola aligned along the X axis (see Fig. 2). This provides a reasonable approximation, although it does cause the corner to be narrowed slightly on approaching the apex. Knowing the subtended angle  $\theta$  means that the locations of the expected boundaries of the perfect sharp corner are known. We constrain the model hyperbola to pass through the intersection of the image window and the corner boundaries. These two points are found as

$$(x_1, y_1) = \begin{cases} (W, \pm W \tan \frac{\theta}{2}) & \text{if } \theta < 90^\circ \\ (\frac{W}{\tan \frac{\theta}{2}}, \pm W) & \text{otherwise} \end{cases}$$

<sup>2</sup> Of course, other distributions that might be produced by oddly shaped corners could produce values outside this range.

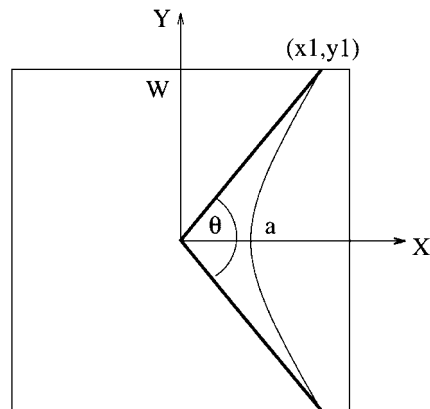


FIG. 2. Modeling a blunt corner with a hyperbola.

so that the implicit equation of the hyperbola is

$$Q(x, y) = x^2 - \frac{x_1^2 - a^2}{y_1^2} y^2 - a^2 = 0.$$

The free parameter  $a$  specifies the distance of the rounded apex from the ideal sharp point of the corner, and increasing values of  $a$  imply increased rounding. The complete model for a blunt model is then

$$\text{corner}(x, y, a) = \begin{cases} \text{foreground} & \text{if } x \geq 0 \text{ and } Q(x, y) \geq 0 \\ \text{background} & \text{otherwise.} \end{cases}$$

Another corner model we have experimented with uses the perfect wedge and replaces the apex by a circular section (Fig. 3). For a circle of radius  $r$  we wish to locate it so that it smoothly joins the straight sections of the corner. This is obtained if the circle is positioned at  $x_c = \frac{r}{m} \sqrt{m^2 + 1}$ , and so the tangent point can be determined:

$$(x_T, y_T) = \left( \frac{x_c}{m^2 + 1}, m x_T \right),$$

where  $\theta$  is the subtended angle and  $m = \tan \frac{\theta}{2}$ . The model is

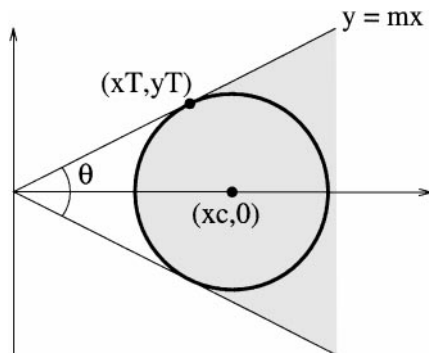


FIG. 3. Modelling a blunt corner with a circular arc.

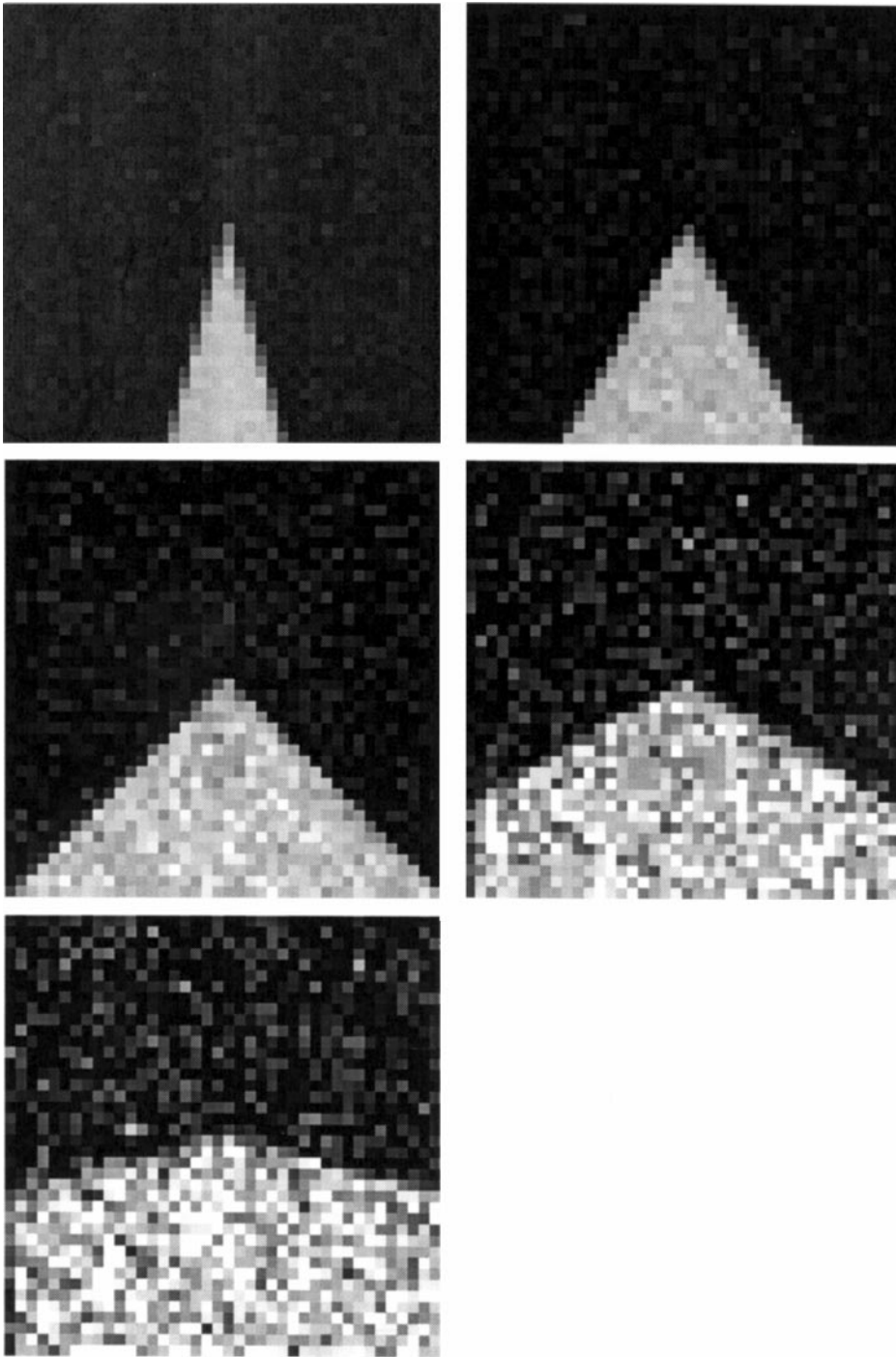


FIG. 4. Sample test corner images.

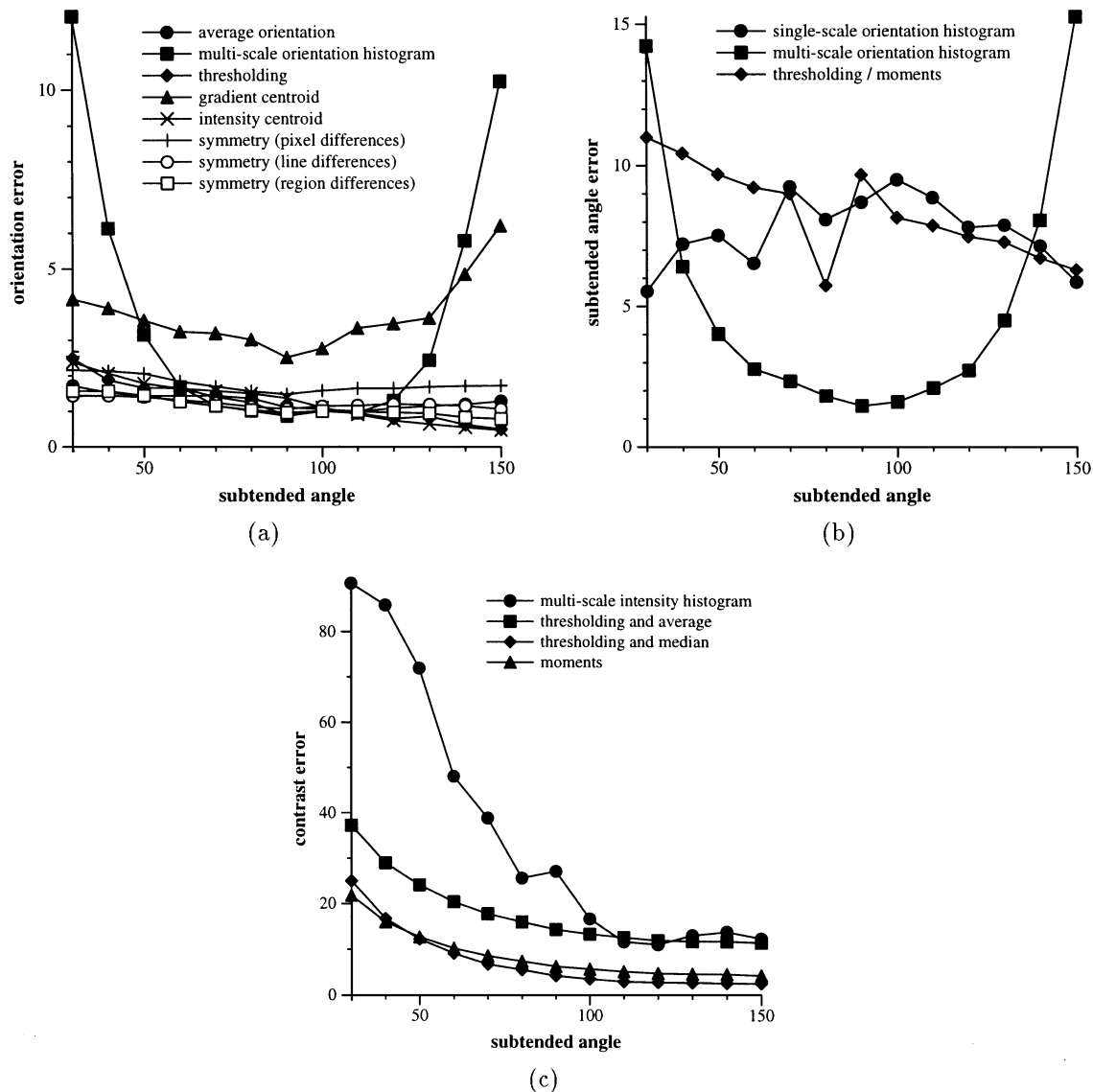


FIG. 5. Effect of subtended angle on measurement accuracy for orientation, subtended angle, and contrast.

then

$$\text{corner}(x, y, r) = \begin{cases} \text{foreground} & \text{if } [x \geq x_T \text{ and } |y| \leq mx] \text{ or} \\ & [(x - x_c)^2 + y^2 \leq r^2] \\ \text{background} & \text{otherwise.} \end{cases}$$

#### 2.4. Boundary Shape

So far we have assumed that corners have straight sides (although possibly a rounded apex). Now we consider curved sides, and distinguish between concave and convex, although the following approach is restricted to symmetric corners; i.e., both sides are either concave or convex. We work with the projection along the corner orientation again. Since the precise shape of the corner boundary is unknown we do not fit a parametric model. Instead we look to see how much the boundary is in-

dentured into or out of the foreground. Each half of the projection along the spatial axis should correspond to one side of the corner. The indentation of each side is measured by dividing the nonzero elements into two halves and fitting straight lines to each. The angle  $\psi$  between the lines then indicates the degree of concavity or convexity. If positive angles are calculated in the counterclockwise direction then the measures are simply

$$\text{concavity} = \frac{\psi}{\text{contrast}}$$

$$\text{convexity} = \frac{-\psi}{\text{contrast}}$$

where large values imply greater curvature. Even though the projection is obtained by integrating the image it may still be

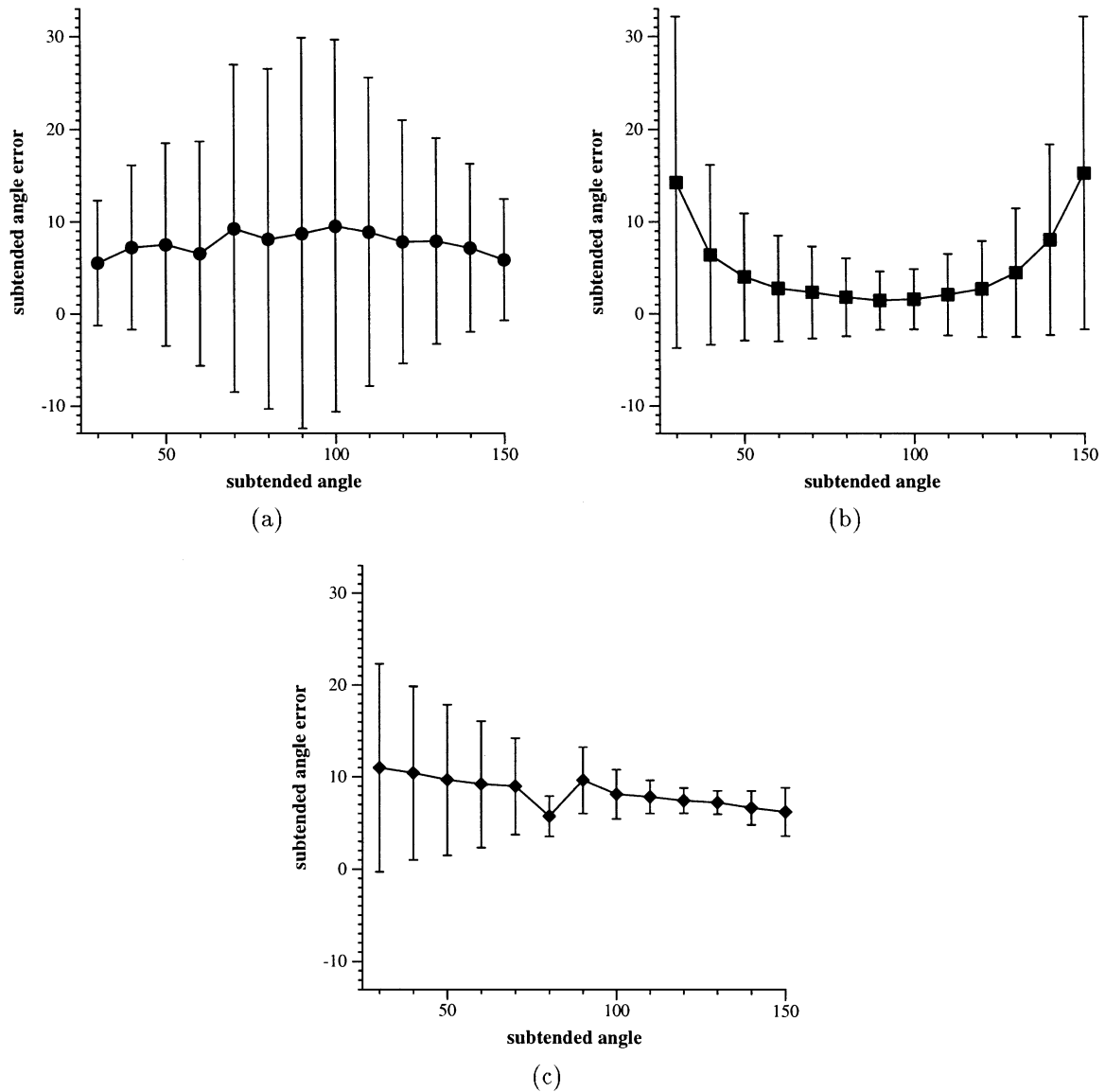


**FIG. 6.** Measurement uncertainty of subtended angle; error bars show one standard deviation; (a) single-scale orientation histogram, (b) multiscale orientation histogram, (c) thresholding/moments.

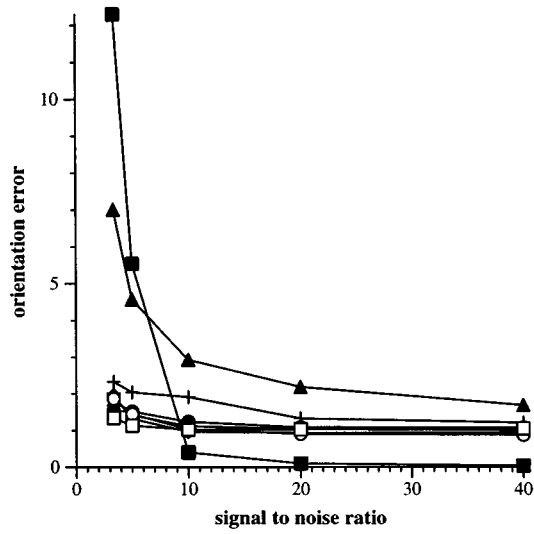
noisy. We therefore require the line fitting to be robust and use the least median of squares (LMedS) method [18].

### 3. RESULTS

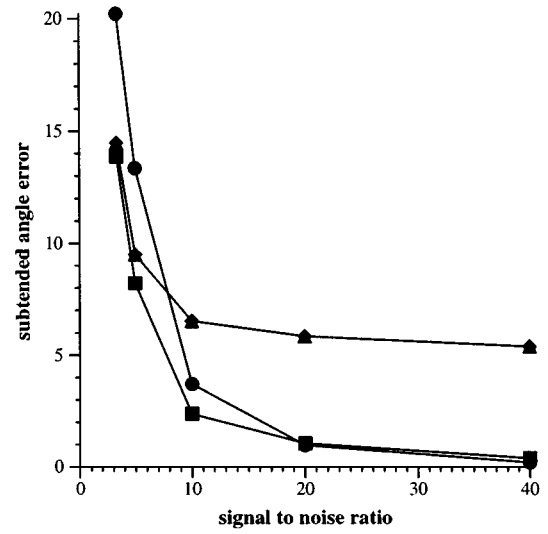
Ideally we would like the methods for measuring corner properties to work reliably over a range of conditions: varying orientations, subtended angles, degrees of noise, etc. To assess the accuracy and robustness of the new methods described here and also some of the previous ones given in [17] they have been extensively tested on synthetic data. Idealized corners were generated for 13 different subtended angles ( $\theta = [30^\circ, 150^\circ]$ ) as  $160 \times 160$  images and then averaged and subsampled down to  $40 \times 40$ . Different levels of Gaussian noise ( $\sigma = [5, 60]$ ) were then re-

peatedly added to create a total of 13,000 test images. Some examples are shown in Fig. 4 with  $\theta = \{30^\circ, 60^\circ, 90^\circ, 120^\circ, 150^\circ\}$  and  $\sigma = \{5, 10, 20, 40, 60\}$ , respectively. The contrast between corner foreground and background was kept constant at 200, so that the images contained signal to noise ratios ranging from 40 to  $3\frac{1}{3}$ . Note that unless otherwise stated all tests use a window size of  $31 \times 31$  and the corner properties were measured at the ideal location: (20, 20).

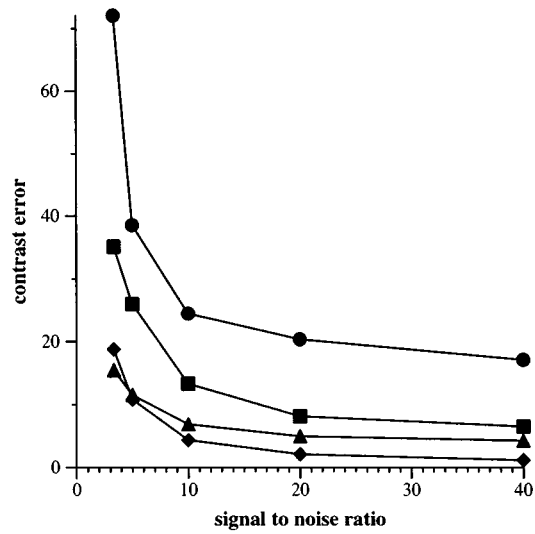
A limitation in the orientation histogram methods for determining orientation and subtended angle as well as the average weighted orientation method for determining orientation described in [17] is that they cannot distinguish between an angle  $\theta$  and its complementary angle  $180^\circ - \theta$ . Although it would be possible to correct this by additional checks we have not pursued



(a)



(b)



(c)

**FIG. 7.** Effect of noise on measurement accuracy for orientation, subtended angle, and contrast.



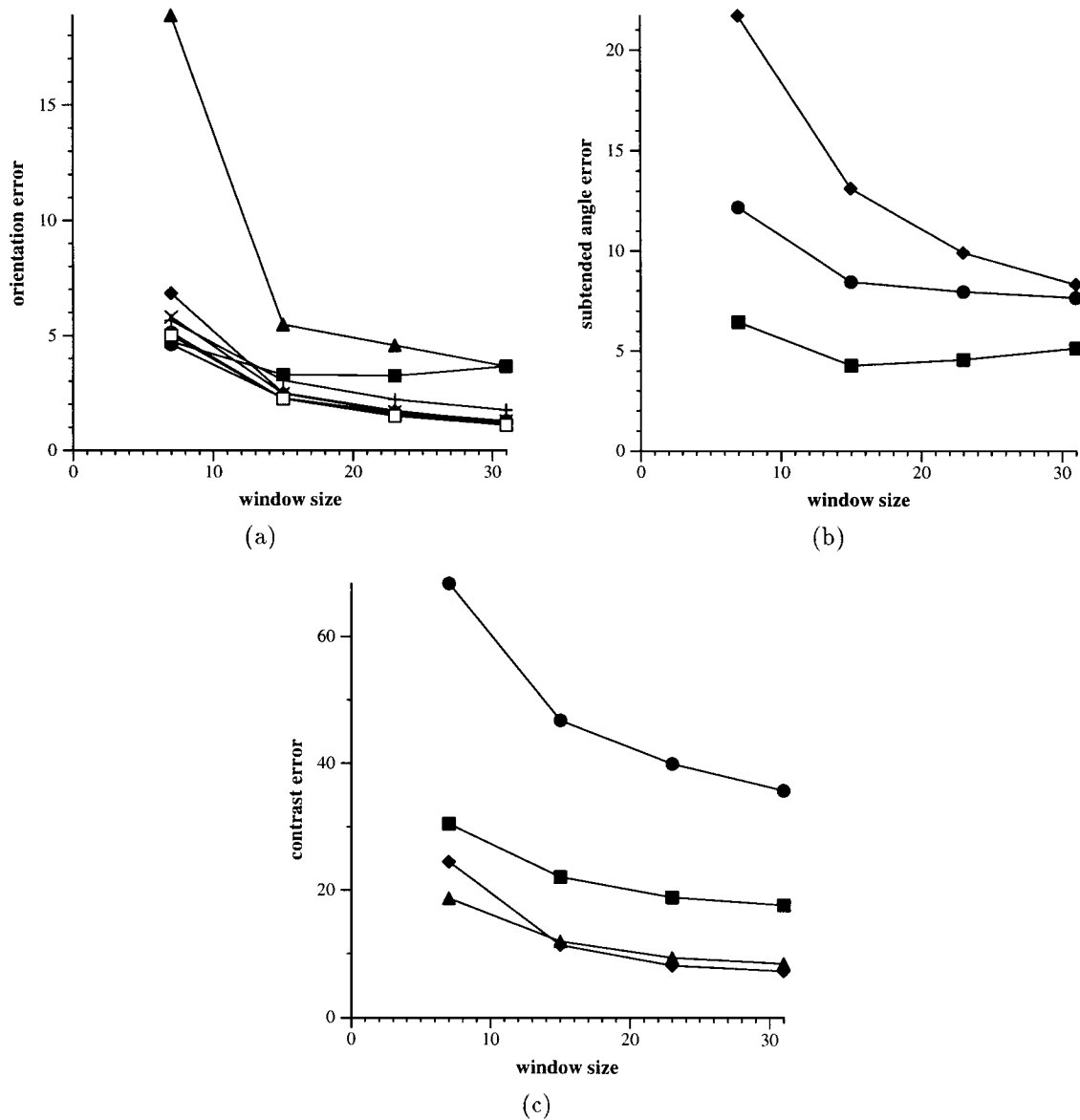


FIG. 8. Effect of window size on measurement accuracy for orientation, subtended angle, and contrast.

that here. However, the results for these methods on the synthetic data have been corrected to account for this problem.

Table 1 shows the error rates of each method averaged over all 13,000 test images. The tests were carried out twice. The first time the corner properties were measured at the known true location of the corner (20, 20). The second time the Kitchen–Rosenfeld [11] detector was applied to the images, and the properties were measured at the corner that was detected closest to the true location. As well as this summary information we also examine the effects of changing each of the image conditions in turn.

### 3.1. Effects of Subtended Angle

Figure 5 shows that the two multiscale orientation histogram methods perform well only around  $90^\circ$  corners. This is to be

expected since they operate on the difference between two orientation peaks—these peaks are most widely separated at  $90^\circ$  since orientations are only measured in the range  $[0^\circ, 180^\circ)$ . It can be concluded that for measuring orientation the multiscale histogram method is only suitable for subtended angles of  $90^\circ \pm 30^\circ$ . The gradient centroid method performs relatively poorly and is also sensitive to subtended angle. The remaining methods are comparable and are relatively insensitive to subtended angle, therefore outperforming the first two methods.

For measuring subtended angles the multiscale orientation histogram method does best at subtended angles of  $90^\circ \pm 40^\circ$ . The other methods are roughly independent of subtended angles, but the graph appears noisy. In particular, the thresholding/moments method has an unexpected dip at  $80^\circ$ . Repeated

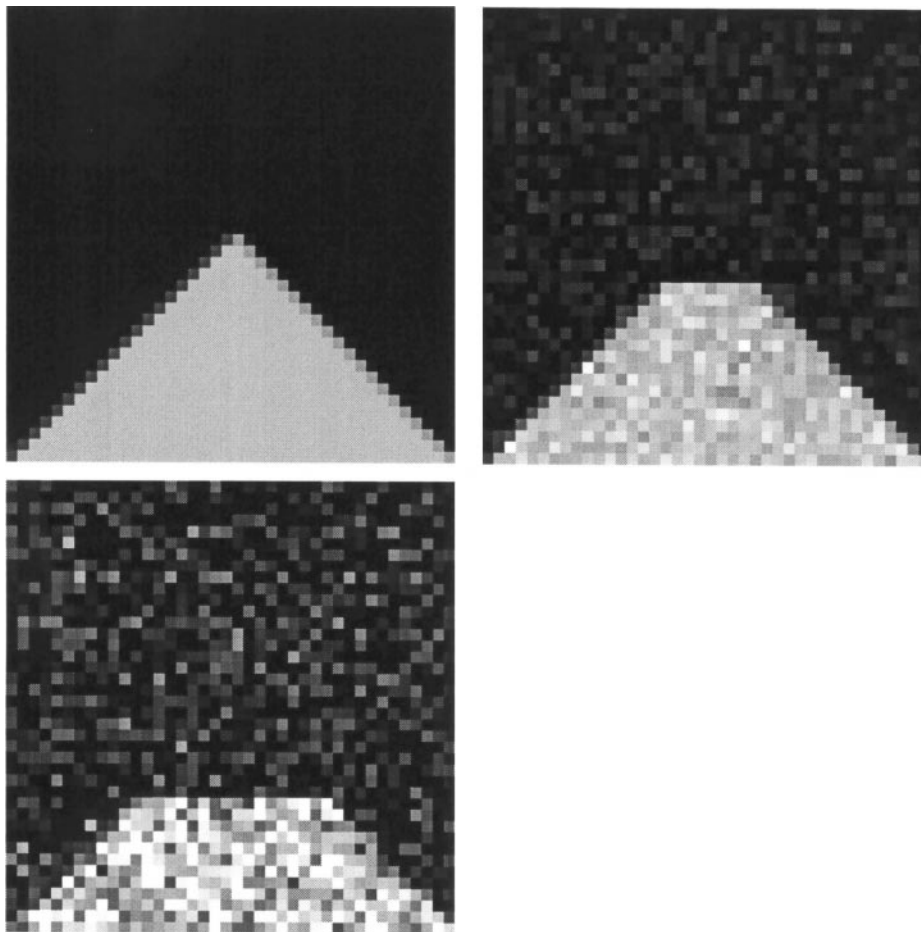


FIG. 9. Sample test corner images with cropping.

tests confirmed this anomaly, and we suggest that it may be an artifact of the digitized synthetic corner. The noisy shape of the single-scale orientation histogram is not surprising when we redraw the performance graph with error bars at  $\pm 1\sigma$  (see Fig. 6a) as there is substantial variability. The lesser variance of the thresholding/moments method does not explain the unexpected dip.

When measuring contrast the multiscale intensity histogram degrades markedly as the subtended angle decreases. This is because at small angles the peak in the histogram corresponding to the corner foreground is small and cannot be identified and located accurately. The other methods degrade more moderately with decreasing subtended angle; thresholding and differencing the medians of the two populations generally performs best.

### 3.2. Effects of Noise

Figure 7 shows the robustness of the methods against increasing amounts of noise. For calculating orientation most methods are fairly insensitive to noise. The major exception is the multiscale orientation histogram method which breaks down dramatically for large amounts of noise. This is caused by the automatic

smoothing technique breaking down, causing the wrong histogram peaks to be selected. The gradient centroid method also degrades significantly. For measuring subtended angles there is less differentiation as all the methods suffer severe degradation. When measuring contrast the multiscale intensity histogram method breaks down again at high levels of noise while the other methods show a somewhat less severe degradation.

### 3.3. Effects of Window Size

Next, we show the effect of changing the window size within which the measures are calculated (see Fig. 8). With the exception of the multiscale orientation histogram increasing the window size provides a moderate improvement in measuring orientation for all methods. In particular, the gradient centroid method performs poorly when a small window is used. For calculating subtended angles an increase in window size again has little effect on the multiscale orientation histogram method, but considerably improves the thresholding/moments method. When calculating contrast increasing window size has most effect on the multiscale orientation histogram and provides a small improvement for the other methods.

### 3.4. Bluntness

Now we look at the effectiveness of the methods for measuring bluntness. Each of the three methods assumes a different model of corner rounding. We cannot therefore generate synthetic blunt corners using any of these models since this would favor the corresponding bluntness measurement method. Instead we blunt the corners by cropping the apex by a straight edge. Examples in Fig. 9 show cropping by 0, 4, and 8 rows of pixels with added noise at  $\sigma = \{0, 20, 60\}$ , respectively. For each degree of cropping 1000 examples of  $90^\circ$  corners containing various amounts of noise were generated for testing. Results are shown in Fig. 10. Both the kurtosis and hyperbola fitting methods do well over a range of degrees of cropping, displaying a fairly linear behavior. The circle fitting method does not fare

so well as it breaks down under large amounts of cropping, losing its linear response, and showing substantial variance. We can quantify the linearity of the methods using Pearson's correlation coefficient. For the kurtosis method we test  $1 - \kappa_N$  against cropping, while for the other two we simply test  $a$  and  $r$ , respectively. The coefficients are 0.98364, 0.98507, and 0.93383, verifying that the first two methods are superior to the third.

### 3.5. Cusps

To test the measurement of concavity and convexity of cusps one synthetic symmetric example was generated of each, and Gaussian noise added as before to provide two sets of 1000 test images. Two instances can be seen in Figs. 11a and 11c.

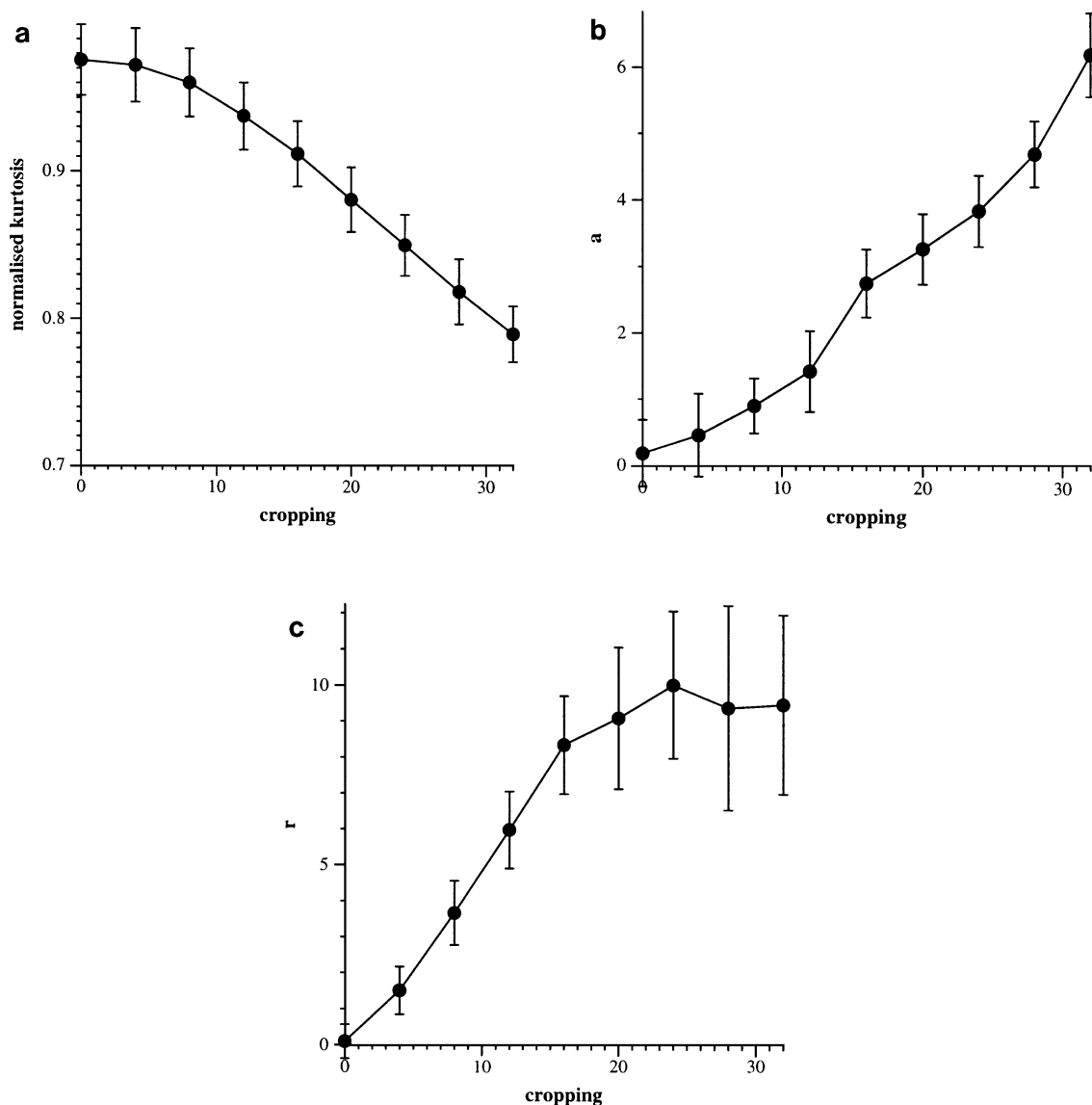


**FIG. 10.** Measuring bluntness. (a) Kurtosis method; (b) hyperbola fitting method; (c) circle fitting method.

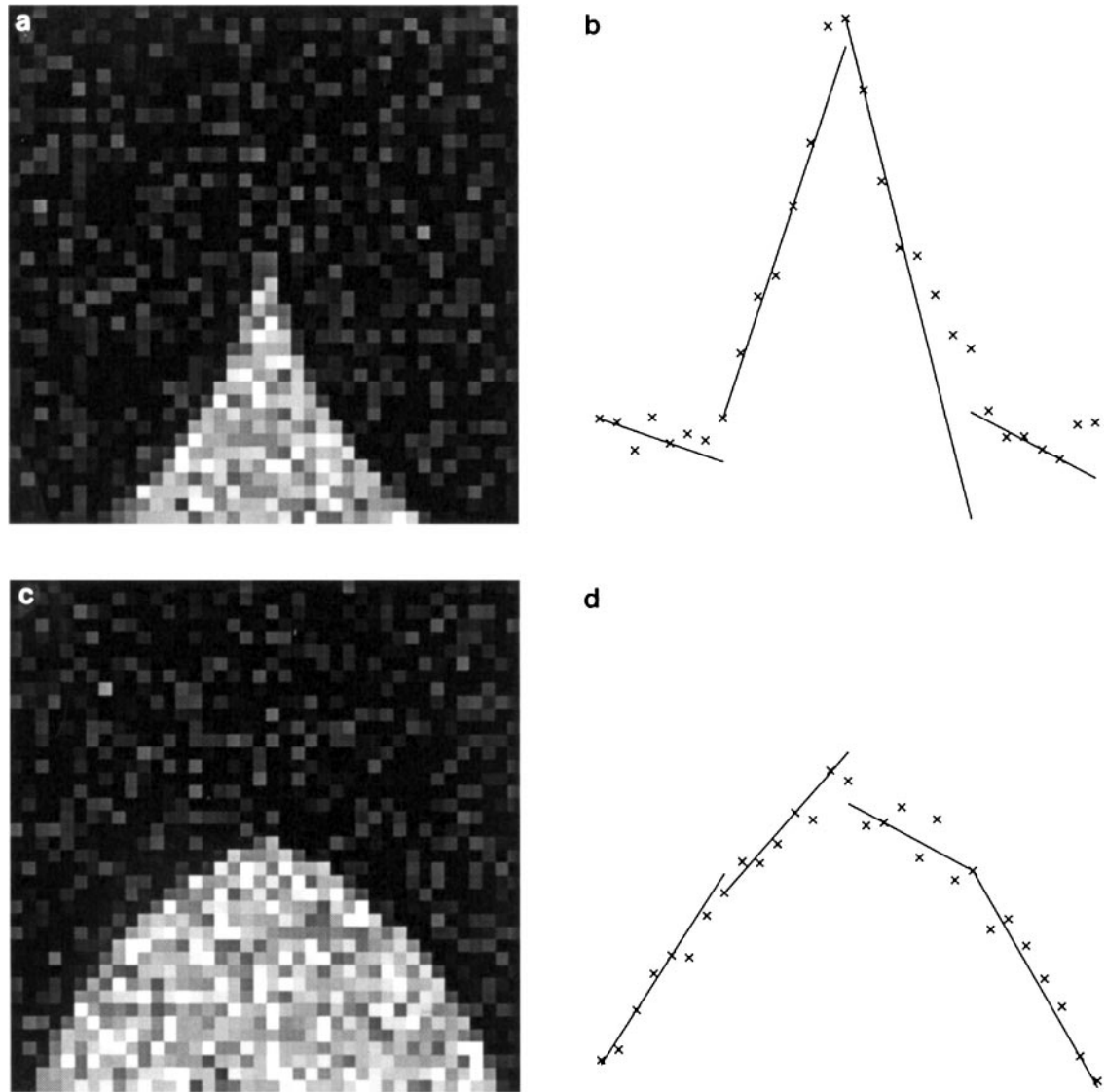


**FIG. 11.** Line fitting for measuring cusp boundary turning angle. (a) Concave corner; (b) lines fitted to projection; (c) Convex corner; (d) lines fitted to projection.

Also shown are the corresponding projections with the lines fitted according to the LMedS criterion. The results of testing the method on test images of each corner type are shown in Fig. 12a. For convenience the spatial axis has been scaled which also causes the angles to be scaled. Even at low S/N ratios the concave and convex corner types can be reliably discriminated. For comparison the method was also tested on 1000 examples of a noisy  $90^\circ$  straight corner. The measured angle is close to zero, allowing it to be confidently classified as a straight edge.

### 3.6. Application to a Real Image

We also show the application of some of the methods to measure corner properties in real images. Since ground truth is not known the results can only be evaluated by eye. Corners are detected using the Kitchen–Rosenfeld detector [11], applying

nonmaximal suppression, and then thresholding based on both the cornerity and edge magnitude value. To reduce the problem of clutter interfering with the measurements a smaller window ( $21 \times 21$ ) is used than for the synthetic images of isolated corners.

Figure 13a shows the selected corners and displays both the orientation (calculated using the thresholding method) and subtended angle (calculated using region symmetry), represented by arcs and radii. Most corners seemed to be correctly characterized although some are rotated by  $180^\circ$  due to the region symmetry occasionally being poorly initialized by the gradient weighted centroid method.

Figure 13b represents corners by circles with radii proportional to contrast. Although variations in contrast are generally small, the results appear reasonable. For instance, inspection shows that the corners of the computer monitor are correctly

about half the contrast of the corners of the black and white rectangle on the wall above it.

Finally, Fig. 13c shows bluntness, again represented by proportionally sized circles. There is little variation in bluntness over the image, corresponding to the uniformity of corners in the scene. Apart from some responses which do not appear to arise from true corners, most corners have a bluntness value between 0.4 and 0.5, caused by quantization and blurring of the corners that were originally sharp in the scene. The remaining corners whose measured bluntness is higher than average appear correct. See, for instance, the bottom lefthand corner of the white square containing the Kaniza triangle.

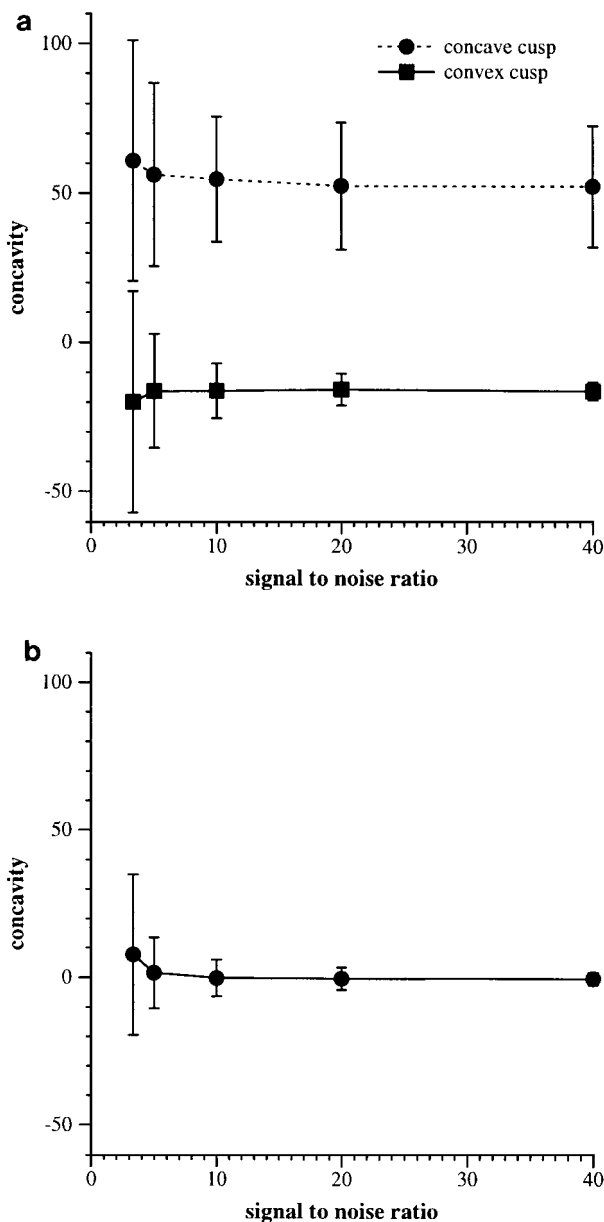


FIG. 12. Effect of noise on measurement accuracy for boundary curvature. (a) Concave and convex cusps; (b) straight boundary corner.

TABLE 1  
Summary of Error Rates for Each Method  
of Measuring Corner Properties

Method	Average error			
	True position		Approximate position	
	$\mu$	$\sigma$	$\mu$	$\sigma$
Orientation				
Average orientation	1.289°	0.949°	1.314°	0.957°
Multi-scale orientation histogram	3.674°	10.552°	3.608°	10.318°
Thresholding	1.223°	1.175°	1.515°	1.795°
Gradient centroid	3.675°	4.090°	4.085°	4.469°
Intensity centroid	1.285°	1.173°	1.629°	1.845°
Symmetry (pixel differences)	1.763°	0.574°	1.976°	1.172°
Symmetry (line differences)	1.224°	0.670°	1.505°	1.406°
Symmetry (region differences)	1.114°	0.755°	1.593°	1.682°
Subtended angle				
Single scale orientation histogram	7.688°	13.653°	7.589°	13.911°
Multi-scale orientation histogram	5.178°	6.416°	5.179°	6.353°
Thresholding	8.353°	4.064°	11.711°	5.165°
Moments	8.353°	4.064°	11.711°	5.165°
Contrast				
Multi-scale intensity histogram	35.898	52.800	34.134	51.851
Thresholding and average	17.816	14.101	17.212	13.751
Thresholding and median	7.443	12.019	6.989	11.667
Moments	8.622	7.459	8.245	7.218

#### 4. CONCLUSIONS

We have described various methods for measuring L-corner properties.<sup>3</sup> In order to compare them they have been extensively tested on synthetic data. This helps demonstrate their strengths and weaknesses and shows under what conditions each method is suitable. Some methods work very well all the time; for instance the thresholding followed by median and the moments methods consistently measure contrast better than the multiscale intensity histogram or thresholding followed by averaging methods. Other methods perform better than others only over a restricted range of conditions. For example, in the range of subtended angles  $90^\circ \pm 40^\circ$  the multiscale orientation histogram method for measuring subtended angle outperforms the other methods, but outside this range it breaks down. Another example is when applying the multiscale orientation histogram method to measure corner orientation. Again it outperforms all the other methods, but breaks down when the signal to noise ratio drops below 10.

Overall, the average orientation, thresholding, intensity centroid, and all the symmetry methods are all good choices for

<sup>3</sup> It should be noted that all these methods make the assumption that the image in the neighborhood of interest is indeed corner-like. Since a standard corner detector is first used to identify such areas then this assumption should be generally valid. If misdetection occurs due to an error in the corner detector then many of the quantities detected would have a totally different meaning.



**FIG. 13.** Corner properties measured from real image. (a) Orientation and angle; (b) contrast; (c) bluntness.



FIG. 13—Continued

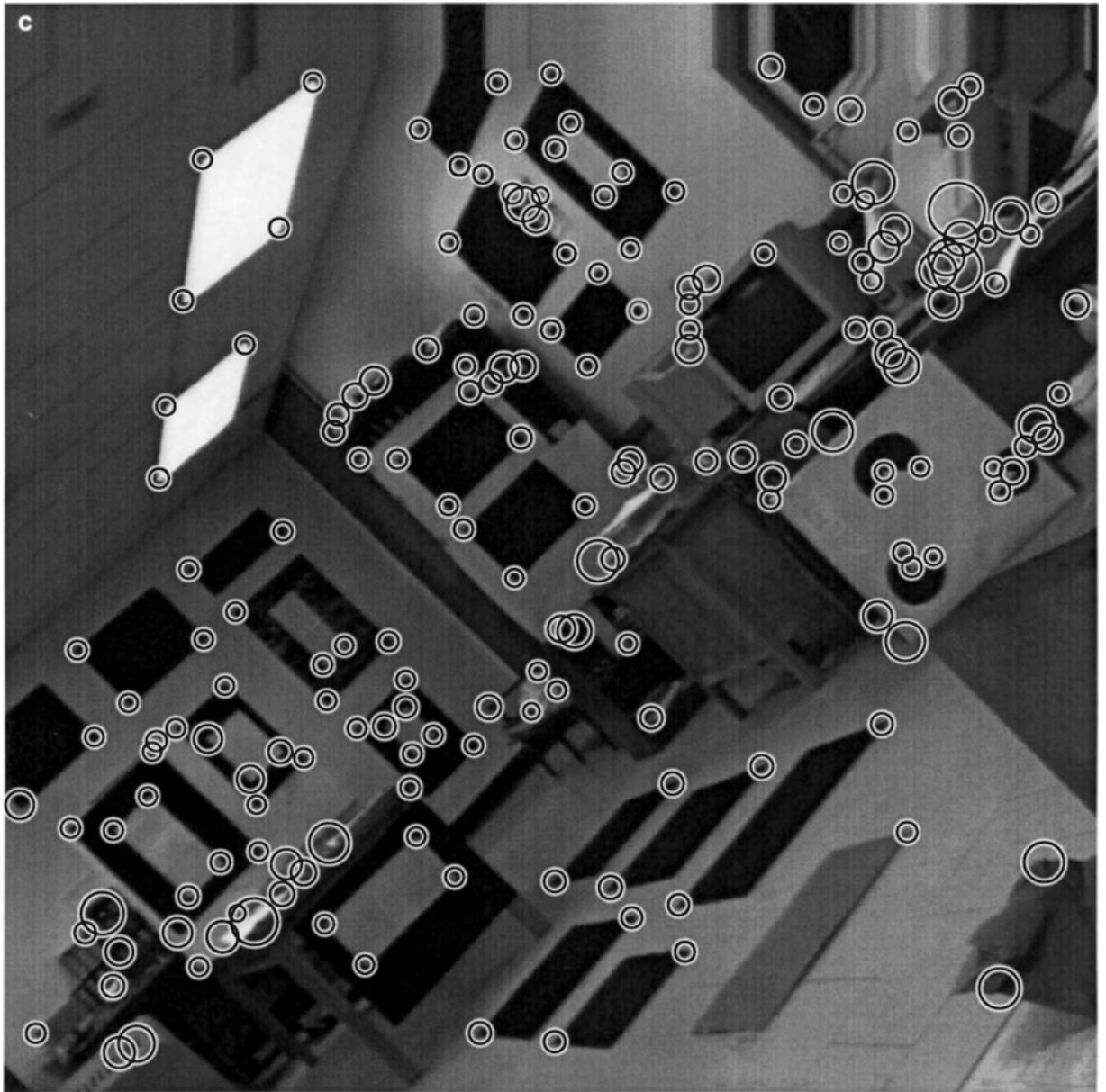


FIG. 13—Continued



measuring orientation. Although it breaks down for very narrow or wide corners the multiscale orientation histogram method is probably the best choice for measuring subtended angle. The thresholding followed by median and the moments methods are best for measuring contrast—the moments method being more robust under severe noise or when a small measurement window is used.

A more limited set of tests has been applied to the methods for measuring bluntness and cusp boundary curvature. For measuring bluntness the kurtosis and hyperbola fitting methods do better than the circle fitting method when the corner is substantially rounded. Finally, the method for measuring boundary shape of cusps worked reliably on the simple test set.

## REFERENCES

1. H. Asada and M. Brady, The curvature primal sketch, *IEEE Trans. Pattern Anal. Mach. Intell.* **8**, 1986, 2–14.
2. S. Baker, S. K. Nayar, and H. Murase, Parametric feature detection. *Int. J. Comput. Vision* **27**, 1998, 27–50.
3. W. F. Bischof and T. Caelli, Parsing scale-space and spatial stability analysis, *Comput. Vision Graphics Image Process.* **42**, 1988, 192–205.
4. T. Blaszkowski and R. Deriche, Recovering and characterizing image features using an efficient model based approach, Technical Report RR-2422, INRIA, 1994.
5. C. H. Chen, J. S. Lee, and Y. N. Sun, Wavelet transformation for gray-level corner detection, *Pattern Recog.* **28**(6), 1995, 853–861.
6. E. R. Davies, Application of the generalized Hough transform to corner detection, *IEEE Proc.* **135**(1), 1988, 49–54.
7. L. S. Davis, Understanding shape: Angles and sides, *IEEE Trans. Comput.* **26**, 1973, 236–242.
8. R. Deriche and G. Giraudon, A computation approach for corner and vertex detection, *Int. J. Comput. Vision* **10**, 1993, 101–124.
9. S. Ghosal and R. Mehrotra, A moment-based unified approach to image feature detection, *IEEE Trans. Image Process.* **6**, 1997, 781–793.
10. A. Guiducci, Corner characterization by differential geometry techniques, *Pattern Recog. Lett.* **8**, 1988, 311–318.
11. L. Kitchen and A. Rosenfeld, Grey-level corner detection, *Pattern Recog. Lett.* **1**, 1982, 95–102.
12. S. T. Liu and W. H. Tsai, Moment preserving corner detection, *Pattern Recog.* **23**, 1990, 441–460.
13. H. Ogawa, Corner detection on digital curves based on local symmetry of the shape, *Pattern Recog.* **22**, 1989, 351–357.
14. W. H. Press, B. P. Flannery, S. A. Teukolsky, and W. T. Vetterling, *Numerical Recipes in C*, Cambridge University Press, Cambridge, UK, 1988.
15. K. Rohr, Recognizing corners by fitting parametric models, *Int. J. Comput. Vision* **9**, 1992, 213–230.
16. P. L. Rosin, Adding scale to corners, in *AI'92—Proc. 5th Aust. Joint Conf. on AI*, pp. 171–176. World Scientific, Singapore, 1992.
17. P. L. Rosin, Augmenting corner descriptors, *Graphical Models Image Process.* **58**(3), 1996, 286–294.
18. P. Rousseeuw and A. Leroy, *Robust Regression and Outlier Detection*, Wiley, New York, 1987.
19. W. H. Tsai, Moment-preserving thresholding: a new approach, *Computer Vision Graphics Image Process.* **29**, 1985, 377–393.
20. Z. Q. Wu and A. Rosenfeld, Filtered projections as an aid in corner detection, *Pattern Recog.* **16**, 1983, 31–38.
21. X. Xie, R. Sudhakar, and H. Zhuang, Corner detection by a cost minimization approach, *Pattern Recog.* **26**, 1993, 1235–1243.
22. W. Zhang and F. Bergholm, Multiscale blur estimation and edge type classification for scene analysis, *Int. J. Comput. Vision* **24**, 1997, 219–250.